Letter

Resummation-based quantum Monte Carlo for quantum paramagnetic phases

Nisheeta Desai [1] and Sumiran Pujari [2,*]

[1]*Department of Theoretical Physics, Tata Institute of Fundamental Research, Mumbai, MH 400005, India*

[2]*Department of Physics, Indian Institute of Technology Bombay, Mumbai, MH 400076, India*

(Received 27 April 2021; revised 15 July 2021; accepted 19 July 2021; published 9 August 2021)

For spin rotational symmetric models with a positive-definite high-temperature expansion of the partition function, a stochastic sampling of the series expansion upon partial resummation becomes logically equivalent to sampling an uncolored closely packed loop-gas model in one higher dimension. Based on this, we devise quantum Monte Carlo updates that importance-sample loop configurations for general $SU(N)$ in fundamental and higher-symmetric representations. The algorithmic performance systematically improves with an increase in (continuous) N, allowing the efficient simulation of quantum paramagnets. The underlying reason for the increased efficacy is the correspondence of quantum paramagnetic phases such as valence bond solids to short-loop phases on the loop-gas side rather than the particular value of N. This also gives a connection between Sandvik's JQ model class and classical loop-gas models in the deconfined universality class.

DOI: 10.1103/PhysRevB.104.L060406

For all areas of physics including strongly correlated matter, efficient computational algorithms are now indispensable. Systematic advances in their design have thus become the keys to progress. Such is exemplarily the case for an important class of algorithms based on the Monte Carlo (MC) method that has provided unbiased insights into multifarious condensed matter systems, as well as lattice gauge theories for elementary particles.

For magnetic insulators that set our backdrop, quantum Monte Carlo (QMC) is now routinely used to study various lattice quantum spin Hamiltonians [1] which provide effective microscopic models for the magnetically active sites in the crystal, or idealized versions aimed at capturing the correct long-distance physics [2]. For these models, an influential set of works [3–8] have set the agenda for charting out the landscape of magnetic and, importantly, quantum non-magnetic phases and associated quantum phase transitions. The large-N perturbative approach of Refs. [3,5–8] offers insights into $SU(2)$ magnets [9], and also connects to quantum dimer models [10] in the $N \to \infty$ limit that serve as effective low-energy models for spin systems [6].

There are two well-known flavors of QMC for simulating these spin models on a d-dimensional lattice at finite temperatures that are extremely efficient for small N. One is based on a path-integral representation in $d+1$ dimensions in (imaginary) time [11,12], and the other based on a stochastic sampling of the high-temperature series expansion (SSE) of the partition function which leads to a discrete $(d+1)$-dimensional formulation [13,14]. Both approaches share a close relation—as a simple example, there is a well-defined spin state on the lattice $(\prod_{i\in\text{lattice}} \otimes |s_i^z\rangle)$ at any point or slice in the additional dimension in both representations—and the ideas in one context may be ported into the other [15]. There are also zero-temperature $(T=0)$ projection-based QMC methods that stochastically project out the ground state from a trial state by exploiting the valence bond basis for antiferromagnetic ground states in the singlet sector [16] including a continuous-N generalization [17].

What has made these methods really powerful is the loop algorithm [12,18–23] and its extensions [24–31] which perform nonlocal updates similar to cluster updates in classical lattice simulations [32,33]. The loop algorithm is based on a colored loop representation of the partition function [34], and changing the color of loops leads to nonlocal updates. This idea can be used in $T=0$ valence bond projector-QMC as well by reintroducing spin variables judiciously in the valence bond formulation as shown by Sandvik and Evertz [23], which also works for Beach *et al.*'s continuous-N generalization [35]. Such loop color updates have also been exploited to study classical loop-gas models [36–38] whose universal properties can parallel that of spin models. This connection goes the other way too, i.e., spin models at finite T may be converted to classical (uncolored) loop models in one higher dimension as noted in "Suzuki-Trotterized" contexts [22,39,40]. This is essentially a resummation over the spin variables.

In this Letter, we design finite-T nonlocal SSE updates based on this resummation which directly handle uncolored loops without any reference to the underlying spin states. This takes advantage of the basic SSE setup which incurs no Suzuki-Trotter errors [41]. These updates lead to a systematic improvement in algorithmic performance as N increases. In relation to the classical loop-gas models alluded to above [36–38], the resultant algorithm is well suited for simulations of phases with predominantly short loops. In fact, this pure loop formulation generalizes the essential idea of valence bond $T=0$ projector-QMC method via the resummation-based updates to simultaneously access both finite temperatures and any total spin sector. More broadly

*sumiran@phy.iitb.ac.in

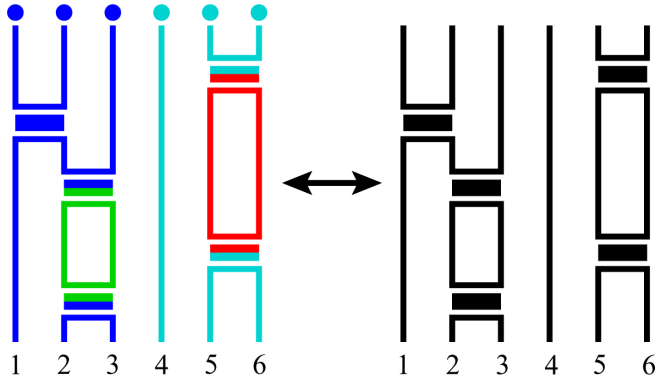

FIG. 1. Illustrative operator string configurations for standard SSE (left) with definite spin states, and for resummed SSE (right) characterized purely by uncolored loops.

speaking, uncolored short loops in space-time are rather the natural objects or building blocks for quantum non-magnetic phases such as valence bond solids (VBSs). These states are of long-standing interest both intrinsically, and for possible proximity to spin-liquid states. On the other hand, colored loops with definite spin states are the natural objects in long-loop phases which correspond to magnetic phases that were exploited by Sandvik-Evertz [23]. We also combine the above with the SSE methods developed by one of the authors in Refs. [42,43] for efficient simulation of higher-symmetric representations of $SU(N)$ that were introduced by Read and Sachdev [6] to expose the myriad possible quantum non-magnetic states for higher spins.

Fundamental representation. We describe the basic idea using the canonical $SU(2)$ spin-$\frac{1}{2}$ nearest-neighbor Heisenberg Hamiltonian on a bipartite lattice. It is

$$H = J \sum_{\langle i,j \rangle} \mathbf{s}_i \cdot \mathbf{s}_j,$$

where $\mathbf{s}_i \equiv (s_i^x, s_i^y, s_i^z)$ are spin-$\frac{1}{2}$ operators on site i at position $\mathbf{r}_i$, and $\langle i, j \rangle$ indexes the nearest-neighbor bonds of the lattice. After a sublattice unitary rotation, $H = -J \sum_{\langle i,j \rangle} H_{ij}$ with the "singlet projector" $H_{ij} = \frac{1}{N} \sum_{\alpha,\beta} |\alpha_i \alpha_j\rangle\langle\beta_i \beta_j|$ up to an innocuous constant. α, β range from 1 to $N = 2$ [44,45]. Then, the high-temperature series representation of the partition function $Z(\beta) = \mathrm{Tr}(e^{-\beta H}) = \sum_n \frac{(-\beta)^n}{n!} \mathrm{Tr}(H^n)$ with $\beta \equiv \frac{1}{kT}$ becomes the (positive-definite) operator-string representation of SSE,

$$\sum_{n=0}^{\infty} \frac{(-\beta)^n}{n!} \sum_{S_n} \sum_{\alpha} \langle \alpha | H_{\{b_1,\mu_1\}} H_{\{b_2,\mu_2\}} \cdots H_{\{b_n,\mu_n\}} | \alpha \rangle,$$

where S_n denotes a string of operator indices, and $\{b_m, \mu_m\}$ is a joint index that tracks for the mth operator in the operator string its bond location $\langle i, j \rangle$ where H_{ij} "lives" via b_m, and whether it is diagonal or off diagonal in the usual choice of s^z basis via μ_m. The operator-string representation thus lives in $d + 1$ dimensions. As remarked earlier, it can be imagined as a configuration of closely packed colored loops [34] as shown in Fig. 1(a). Now, one may resum over the spin or color values of these closely packed loops without breaking or changing any loop connections in the operator string. This then renders the ensemble as a configuration of closely packed uncolored loops as shown in Fig. 1(b). This loop-gas representation for the high-temperature series may be written as

$$Z(\beta) = \sum_{n=0}^{\infty} \frac{(-\beta)^n}{n!} N^{n_l} \sum_{S_n} h_{b_1} h_{b_2} \cdots h_{b_n}, \tag{1}$$

where bond index b_i is now the only indexing required, h_{b_i} indicates the spin-symmetric matrix element contribution ($-\frac{J}{N}$ in our example) at b_i, and n_l is the number of loops in a given configuration.

We may suggestively rewrite the above as $Z = \sum_{\{C_{\mathrm{loops}}\}} W(C_{\mathrm{loops}})$, where C_{loops} is any allowed closely packed uncoloured loop-gas configuration with only one underlying operator where loops abut each other at various time slices [Fig. 1(b)], and $W(C_{\mathrm{loops}}) = \frac{(\beta J/N)^n}{n!} N^{n_l}$. The underlying operators thus perform the role of "transfer matrices" in the loop-gas language [36]. The uncolored nature of the loop gas emerges in the presence of $SU(N)$ symmetry, which ensures that the diagonal and off-diagonal operators contribute the same factor to the weight of the configuration. Having done the resummation though, N is now purely a parameter and can be any positive, real number. It also gets rid of the index which tracks diagonal versus off-diagonal operators, which implies a superposition of spin states at any time slice.

Estimators. The simplest QMC estimator is energy, and it is measured in the same way here as in standard SSE. This is because, if we now color back the uncolored loops, the contribution to the energy estimator is *independent* of the coloring, i.e., each coloring contributes the same value ($\frac{n}{\beta}$) to the energy estimator [15]. The measurement of bond operators also remains unchanged, e.g., $B_\lambda(\vec{r}) \equiv \mathbf{s}_\mathbf{r} \cdot \mathbf{s}_{\mathbf{r}+\hat{e}_\lambda}$ on the square lattice. We can similarly measure the square lattice VBS order parameters, $\phi_x = \frac{1}{N_s} \sum_\mathbf{r} (-1)^{r_x} \langle B_x(\mathbf{r}) \rangle$ and $\phi_y = \frac{1}{N_s} (-1)^{r_y} \langle B_y(\mathbf{r}) \rangle$. Measuring the correlations of the bond operator $\tilde{C}_{\phi_\lambda^2}(\mathbf{r}) = \langle B_\lambda(\mathbf{0}) B_\lambda(\mathbf{r}) \rangle$ is also straightforward. The estimator of the spin stiffness which tracks magnetic ordering is changed due to the resummation. In standard SSE, the stiffness is related to the winding of colored loops according to the following relation, $\rho = \frac{\langle \mathcal{W}_c^2 \rangle}{\beta}$, where $\langle \mathcal{W}_c^2 \rangle$ is the winding fluctuations of colored loops [15]. It is related to the winding fluctuations of uncolored loops as $\langle \mathcal{W}_u^2 \rangle = \frac{N^2}{(N-1)} \langle \mathcal{W}_c^2 \rangle$, which gives an "improved" estimator for the stiffness:

$$\rho = \frac{(N-1)}{N^2} \frac{\langle \mathcal{W}_u^2 \rangle}{\beta}. \tag{2}$$

The derivation of the winding fluctuation relation is given in Ref. [46]. This estimator for stiffness can be used in standard SSE as well.

Implementation and application. Based on Eq. (1), we implement a Monte Carlo algorithm to directly sample the uncolored loop ensemble. Each MC update consists of proposing to insert a spin-symmetric operator at an "identity" location or to remove an already existing "non-identity" spin-symmetric operator at various space-time locations. The proposals get accepted with Metropolis probabilities which are governed by the change $n \to n \pm 1$ (for the Heisenberg model) and the change in the number of loops $\delta(n_l)$ [46]. For H_{ij}, $\delta(n_l)$

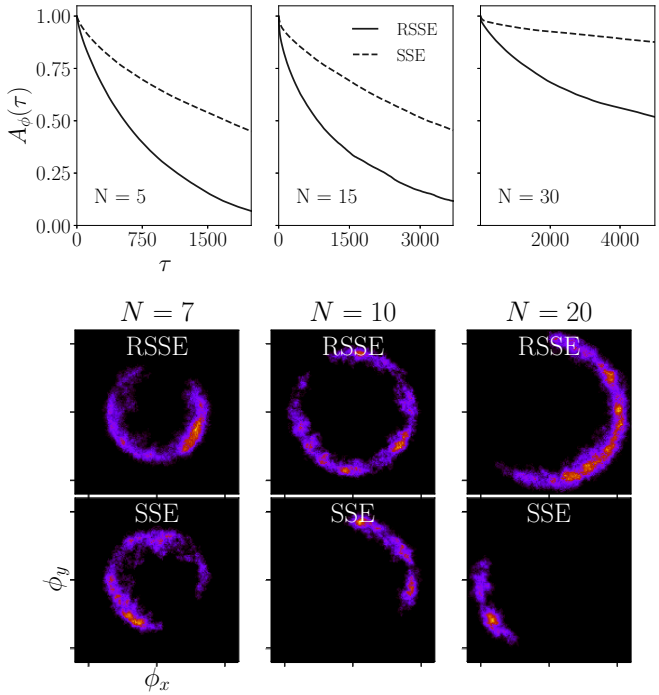

FIG. 2. Top: Comparison of autocorrelation of the VBS order parameter ($\phi = \sqrt{\phi_x^2 + \phi_y^2}$) on a 16×16 lattice for $N = 5, 15, 30$ at $\beta = 128, 64, 64$, respectively, measured after each Monte Carlo step using the resummation algorithm with that of the standard SSE. Autocorrelations fall off faster in the resummed SSE (RSSE) algorithm systematically as N increases. These values of N correspond to the short-loop or VBS phase [47] showing the efficacy of resummation-based updates for short-loop phases in general. Bottom: Joint histograms of the VBS order parameters, ϕ_x and ϕ_y, for $N = 7, 10, 20$, on a 16×16 lattice at $\beta = 128, 128, 64$, respectively. ϕ_x and ϕ_y have been measured at every Monte Carlo step for 10^6 steps. For $N = 7$, the performances of both algorithms are comparable. However, as we go deeper into the VBS phase for higher values of N, we clearly see that resummed SSE (RSSE) spans the angular space of the histogram better, thus proving to be the more ergodic algorithm in this regime.

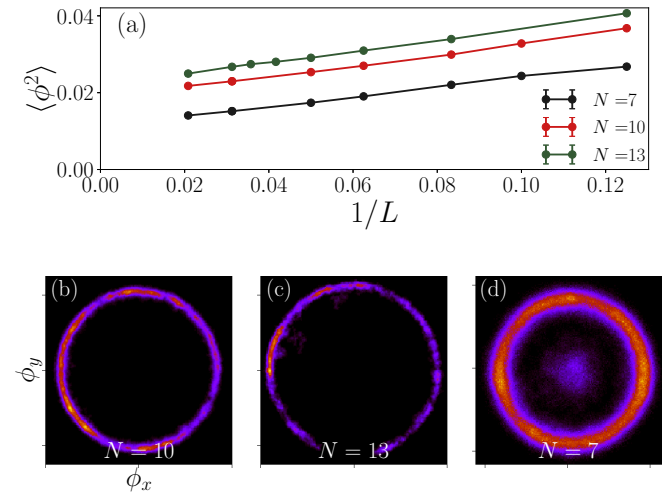

FIG. 3. (a) Finite-size scaling of the VBS order parameter for the $SU(N)$ square lattice antiferromagnet in the fundamental representation for $N = 7, 10, 13$ at $\beta = 128$ representative of zero-temperature limit [46,49]. It clearly extrapolates to finite values showing VBS order in this regime as is expected [47]. Bottom: The joint histogram of ϕ_x and ϕ_y measured at every tenth Monte Carlo step with a total of 10^7 steps. (b), (c) At low enough temperatures, the histograms show $U(1)$ symmetry for $N = 10, 13$ (at $\beta = 128, 256$, respectively) on a 32×32 lattice. (d) For $N = 7$, at $\beta = 64$ on a 16×16 lattice, the distribution peaks at an $U(1)$ symmetric ring and at $\phi_x = \phi_y = 0$ suggesting a first-order transition.

takes only the values ± 1 purely due to considerations of loop topology.

One may anticipate improved performance as N increases compared to standard SSE: In any (typical) instance of the standard SSE operator string configuration, the off-diagonal operator contributions start to dominate those of diagonal operators as N increases. This is simply due to there being $N(N-1)$ off-diagonal operators versus N diagonal operators in H_{ij}. This makes the "diagonal" update of standard SSE—that changes n by inserting or removing diagonal operators between two (identical) definite spin states—less efficient in updating the operator string (the "off-diagonal" update of standard SSE changes only the spin or color value of the loop as remarked earlier, and does not change n). This is a non-issue in our algorithm; operators can be potentially inserted or removed at any space-time location. This improved performance is indeed seen as discussed in Fig. 2. From a loop-gas perspective on the other hand, the resummed SSE algorithm is apt for simulating any phase with predominantly short loops where the computation of $\delta(n_l)$ becomes quite efficient. This is the underlying reason to prefer resummed SSE for short-loop phases (regardless of N) such as VBSs (Fig. 2) as mentioned earlier. This should apply for other non-magnetic phases such as the plaquette VBS or the Haldane-nematic phase [7,48]. These updates can also supplement the standard SSE diagonal and loop updates in long-loop phases or near transitions if needed for performance.

We now apply the resummed SSE algorithm to the square lattice antiferromagnet, $H = -\frac{J}{N} \sum_{\langle ij \rangle} \sum_{\alpha,\beta=1}^{N} |\alpha_i \alpha_j\rangle\langle \beta_i \beta_j|$, for several N. In the fundamental representation, it maps to the non-interacting quantum dimer model (QDM) with one dimer per vertex as $N \to \infty$ [6]. Only very recently, an efficient algorithm based on SSE has been developed for finite-T simulations directly in the constrained Hilbert space of the QDM [50]. We can also access the large-N regime in our simulations efficiently. In Fig. 3(a), we see VBS order at low enough temperatures in this regime. However, we see $U(1)$-symmetric VBS order histograms as shown in Figs. 3(b) and 3(c) in contrast to the "mixed" phase histograms of Ref. [51] for similar system sizes. The approach to the constrained Hilbert space of QDM in the loop-gas representation can also be quantified as shown in the final section of Ref. [46]. We find non-negligible deviations from QDM Hilbert space to put $SU(N)$ magnets away from the perturbative neighborhood of QDM even for quite large N. We ascribe this to the contrast between our results and Ref. [51]—a relevant detail on the connection between $SU(N)$ magnets and QDM. Figure 3(d) shows how the algorithm performs near the thermal transition out of the ordered phase.

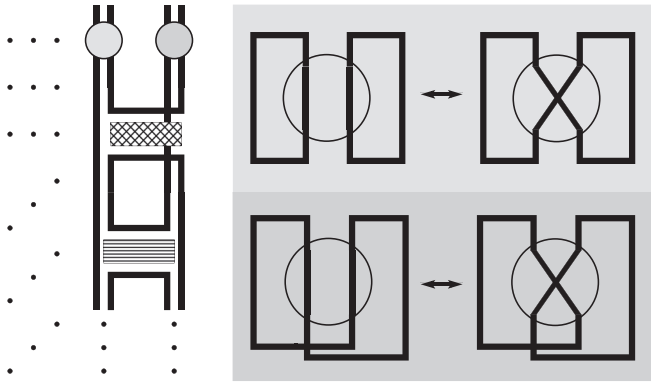

FIG. 4. Schematic to illustrate the resummation over the projection operators. On the left side is shown a small section of the uncolored loop QMC configuration with two split-spins per site. On the right is shown the rewiring MC update at the projection time slice. The shade of gray corresponds to the projection operators shown as circles in the QMC configuration on the left, assuming a loop geometry without any other operators on the shown bond elsewhere in time.

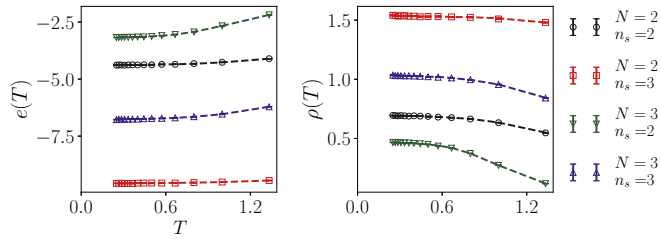

FIG. 5. Comparison of finite-temperature energy per unit site $e(T)$ and spin stiffness $\rho(T)$ measured in our algorithm with standard SSE (dashed lines) on a 4×4 lattice for several N and n_s (number of split-spins or symmetric flavors) [49].

Higher-symmetric representations. We now write down resummation-based updates for higher representations by making use of the "split-spin" language [40,42,52,53] which splits $\mathbf{S}_i$ as $\mathcal{P}_i(\sum_{a=1}^{2S} \mathbf{s}_{i,a})\mathcal{P}_i$, where $\mathcal{P}_i$ are appropriate projection operators to stay in the correct Hilbert space. We take the spin-1 Heisenberg model for $SU(2)$ as our example, which automatically extends to the $SU(N)$ case with two symmetric "flavors." The spin-1 Heisenberg model $H = J\sum_{\langle i,j\rangle}(\mathbf{S}_i \cdot \mathbf{S}_j)$ in the split-spin language is written as $H = \mathcal{P}\tilde{H}\mathcal{P}$ with $\tilde{H} = J\sum_{\langle i,j\rangle}\sum_{a,b}\mathbf{s}_{i,a}\cdot\mathbf{s}_{j,b}$ and a, b is now a split-spin index running over the number of symmetric flavors. $\mathcal{P}$ is a projection operator that projects onto fully symmetric subspace over the split-spins, i.e., $\mathcal{P} = \prod_i \mathcal{P}_i$ and $\mathcal{P}_i \equiv |\uparrow\uparrow\rangle\langle\uparrow\uparrow| + |\downarrow\downarrow\rangle\langle\downarrow\downarrow| + (\frac{|\uparrow\downarrow\rangle+|\downarrow\uparrow\rangle}{\sqrt{2}})(\frac{\langle\uparrow\downarrow|+\langle\downarrow\uparrow|}{\sqrt{2}})$ for the two split-spins on the ith site. With this in hand, the standard-SSE operator-string representation follows from $Z(\beta) = \mathrm{Tr}_{\mathbf{S}}(e^{-\beta H}) = \mathrm{Tr}_{\mathbf{s}}(e^{-\beta\tilde{H}}\mathcal{P})$. To ensure symmetrization, it is enough that the projection operator acts at one particular time slice [52]. We may now resum as before to get a configuration in terms of uncolored loops with, in this case, two "parallel" loops running at each space-time point as sketched on the left side of Fig. 4. The resummation over colors proceeds exactly the same as before to give the N^{n_l} reweighting factor.

To resum over the projection operator, one must ensure that the action of the projection operator $\mathcal{P}_i$ is faithfully captured on all sites. In standard SSE, one implements the projection by the use of a directed loop update [25,27] at the projection time slice [54]. Resumming over this now amounts to a "rewiring" of the two uncolored loops at the two split-spin sites at this time slice as shown on the right side of Fig. 4. So, the implementation essentially mimics that of the earlier section with an extra MC update for the projection time slice where one proposes to reconfigure the split-spin connections as in Fig. 4 with the acceptance probability again governed by the $\delta(n_l)$ due to this proposal [46]. Extending this to yet higher-symmetric representations follows along very similar lines with more split-spins per site. In Fig. 5, we demonstrate the implementation of these extensions by benchmarking energy and spin stiffness with standard SSE. Simulations of $SU(N)$ models in these higher-symmetric representations have previously been carried out using colored loop updates [55,56]. Our algorithm provides an alternative to this that can allow more efficient access to the quantum non-magnetic states of $SU(N)$ antiferromagnets [6,7], thereby opening up further studies on (quantum) phase transitions with N and T [57].

Discussion. One may finally ask if there is a physical meaning to the uncolored loops, or are they just algorithmic constructs. Any such interpretation, apart from providing intuition, can help formulate other useful QMC estimators [58] based on our generalization of the valence bond $T = 0$ projector-QMC method to finite T without the singlet sector restriction. We can indeed interpret them as follows: At a colored level in standard SSE, an operator $|\alpha_i\alpha_j\rangle\langle\beta_i\beta_j|$ destroys β_i, β_j in a state ("below" the operator in Fig. 1) and creates α_i, α_j in the resultant state ("above" the operator). Thus, $|\alpha_i\alpha_j\rangle\langle\beta_i\beta_j| \equiv b^\dagger_{i,\alpha}b^\dagger_{j,\alpha}b_{i,\beta}b_{j,\beta}$, where $b, b^\dagger$ stand for the destruction and creation operations, respectively. If $\chi_{ij,\alpha} \equiv b_{i,\alpha}b_{j,\alpha}$, then an α-colored loop is of the form $\chi^\dagger_{li,\alpha}\cdots\chi^\dagger_{jk,\alpha}\chi_{ij,\alpha}$. Therefore, upon resumming, an uncolored loop has the following $SU(N)$-symmetric operator content, $\tilde{\chi}^\dagger_{li}\cdots\tilde{\chi}^\dagger_{jk}\tilde{\chi}_{ij}$ with $\tilde{\chi}_{ij} = \sum_\alpha \chi_{ij,\alpha}$. A similar interpretation in the "reverse" direction from loops to magnetic degrees of freedom was laid down by Nahum *et al.* in Refs. [36,37,59], but the Hamiltonian does not take a simple form for three-dimensional (3D) loop gases [60]. Resummation instead gives a recipe to go from local Hamiltonians to loop-gases including for higher-symmetric representations.

The above interpretation gives a connection between the 2D JQ models [2,61] and the 3D loop-gas model studied by Nahum *et al* in Ref. [38], both of which have been argued to exhibit deconfined criticality [62,63]. The Q term—a tensor product of several singlet projectors over independent bonds $\prod_{i=1}^{p} H_{b_i}$—gives an additional rule for how loops may abut each other on a given time slice. A Q operator in the uncolored loop representation will lead to p loop abutments at a given time slice of the layered extension of the underlying lattice, just as each H_b led to one loop abutment as in Fig. 1. The J, Q terms in the loop-gas language thus define appropriate transfer matrices. This throws a "forward" perspective on Refs. [38,64], in that by resumming, any spin-symmetric

Hamiltonian with a positive-definite high-temperature series expansion exhibiting deconfined criticality implies the same between a long-loop and a short-loop phase in a logically equivalent loop gas.

We thank F. Alet, K. Damle, and R. Kaul for discussions. We especially thank K. Damle for a critical reading and feedback on the manuscript. The numerical results were obtained using the computational facilities (Chandra cluster) of the Department of Physics, IIT Bombay. N.D. was partially supported by NSF Grant No. DMR-1611161, and partially by a National Postdoctoral Fellowship of SERB, DST, Government of India (PDF/2020/001658) at the Department of Theoretical Physics, TIFR. S.P. was supported by IRCC, IIT Bombay (17IRCCSG011) and SERB, DST, India (SRG/2019/001419).

[1] A. W. Sandvik, in *Many-Body Methods for Real Materials*, edited by E. Pavarini, E. Koch, and S. Zhang, Lecture Notes of the Autumn School on Correlated Electrons 2019, Schriften des Forschungszentrums Jülich: Modeling and Simulation Vol. 9 (Forschungszentrum Jülich GmbH Zentralbibliothek, Jülich, 2019), pp. 16.1–16.32.
[2] R. K. Kaul, R. G. Melko, and A. W. Sandvik, Annu. Rev. Condens. Matter Phys. **4**, 179 (2013).
[3] I. Affleck, Phys. Rev. Lett. **54**, 966 (1985).
[4] F. D. M. Haldane, Phys. Rev. Lett. **61**, 1029 (1988).
[5] N. Read and S. Sachdev, Phys. Rev. Lett. **62**, 1694 (1989).
[6] N. Read and S. Sachdev, Nucl. Phys. B **316**, 609 (1989).
[7] N. Read and S. Sachdev, Phys. Rev. B **42**, 4568 (1990).
[8] N. Read and S. Sachdev, Phys. Rev. Lett. **66**, 1773 (1991).
[9] Also, $SU(N)$ or, more generally, $SU(2) \bigotimes SU(M)$, arise physically for Kugel-Khomskii models with both spin and orbital degrees of freedom, and other contexts with additional internal quantum numbers. The (algorithmic) ideas of this Letter extend to these models as well.
[10] D. S. Rokhsar and S. A. Kivelson, Phys. Rev. Lett. **61**, 2376 (1988).
[11] M. Suzuki, S. Miyashita, and A. Kuroda, Prog. Theor. Phys. **58**, 1377 (1977).
[12] B. B. Beard and U.-J. Wiese, Phys. Rev. Lett. **77**, 5130 (1996).
[13] A. W. Sandvik and J. Kurkijärvi, Phys. Rev. B **43**, 5950 (1991).
[14] A. W. Sandvik, J. Phys. A: Math. Gen. **25**, 3667 (1992).
[15] A. W. Sandvik, in *Lectures on the Physics of Strongly Correlated Systems XIV: Fourteenth Training Course in the Physics of Strongly Correlated Systems*, edited by A. Avella and F. Mancini, AIP Conf. Proc. Vol. 1297 (AIP, Melville, NY, 2010), pp. 135–338.
[16] A. W. Sandvik, Phys. Rev. Lett. **95**, 207203 (2005).
[17] K. S. D. Beach, F. Alet, M. Mambrini, and S. Capponi, Phys. Rev. B **80**, 184401 (2009).
[18] H. G. Evertz, G. Lana, and M. Marcu, Phys. Rev. Lett. **70**, 875 (1993).
[19] H.-P. Ying, U.-J. Wiese, and D.-R. Ji, Phys. Lett. A **183**, 441 (1993).
[20] N. Kawashima and J. E. Gubernatis, Phys. Rev. Lett. **73**, 1295 (1994).
[21] A. W. Sandvik, Phys. Rev. B **59**, R14157(R) (1999).
[22] H. G. Evertz, Adv. Phys. **52**, 1 (2003).
[23] A. W. Sandvik and H. G. Evertz, Phys. Rev. B **82**, 024407 (2010).
[24] N. V. Prokof'ev, B. V. Svistunov, and I. S. Tupitsyn, J. Exp. Theor. Phys. **87**, 310 (1998).
[25] O. F. Syljuåsen and A. W. Sandvik, Phys. Rev. E **66**, 046701 (2002).
[26] A. W. Sandvik, Phys. Rev. E **68**, 056701 (2003).
[27] F. Alet, S. Wessel, and M. Troyer, Phys. Rev. E **71**, 036706 (2005).
[28] D. Heidarian and K. Damle, Phys. Rev. Lett. **95**, 127206 (2005).
[29] S. V. Isakov, S. Wessel, R. G. Melko, K. Sengupta, and Y. B. Kim, Phys. Rev. Lett. **97**, 147202 (2006).
[30] R. G. Melko, J. Phys.: Condens. Matter **19**, 145203 (2007).
[31] S. Biswas, G. Rakala, and K. Damle, Phys. Rev. B **93**, 235103 (2016).
[32] R. H. Swendsen and J.-S. Wang, Phys. Rev. Lett. **58**, 86 (1987).
[33] U. Wolff, Phys. Rev. Lett. **62**, 361 (1989).
[34] R. K. Kaul, Phys. Rev. B **91**, 054413 (2015).
[35] See footnote [19] of Beach *et al.* [17], and the associated text.
[36] A. Nahum, J. T. Chalker, P. Serna, M. Ortuño, and A. M. Somoza, Phys. Rev. Lett. **107**, 110601 (2011).
[37] A. Nahum, J. T. Chalker, P. Serna, M. Ortuño, and A. M. Somoza, Phys. Rev. B **88**, 134411 (2013).
[38] A. Nahum, J. T. Chalker, P. Serna, M. Ortuño, and A. M. Somoza, Phys. Rev. X **5**, 041048 (2015).
[39] M. Aizenman and B. Nachtergaele, Commun. Math. Phys. **164**, 17 (1994).
[40] N. Kawashima and J. E. Gubernatis, J. Stat. Phys. **80**, 169 (1995).
[41] M. Suzuki, Prog. Theor. Phys. **56**, 1454 (1976).
[42] N. Desai and R. K. Kaul, Phys. Rev. Lett. **123**, 107202 (2019).
[43] N. Desai, Ph.D. thesis, University of Kentucky, Lexington,2020.
[44] R. K. Kaul, Phys. Rev. B **84**, 054407 (2011).
[45] Formally, for $N > 2$, the magnetic degrees of freedom are in the fundamental representation on one sublattice, while they are in the conjugate-to-fundamental representation on the other sublattice. See, e.g., Ref. [44].
[46] See Supplemental Material at http://link.aps.org/supplemental/10.1103/PhysRevB.104.L060406 for further details on the implementation of the resummation-based updates, and some other technical details, where the final section discusses the approach to the quantum dimer model Hilbert space in the large-N regime for the uncolored loop representation.
[47] K. Harada, N. Kawashima, and M. Troyer, Phys. Rev. Lett. **90**, 117203 (2003).
[48] I. Affleck, T. Kennedy, E. H. Lieb, and H. Tasaki, Commun. Math. Phys. **115**, 477 (1988).
[49] The errors on the data points are smaller in size than the symbols representing them, and are hence not explicitly visible in the plots.
[50] Z. Yan, Y. Wu, C. Liu, O. F. Syljuåsen, J. Lou, and Y. Chen, Phys. Rev. B **99**, 165135 (2019).

[51] Z. Yan, Z. Zhou, O. F. Syljuåsen, J. Zhang, T. Yuan, J. Lou, and Y. Chen, Phys. Rev. B **103**, 094421 (2021).
[52] S. Todo and K. Kato, Phys. Rev. Lett. **87**, 047203 (2001).
[53] N. Kawashima and K. Harada, J. Phys. Soc. Jpn. **73**, 1379 (2004).
[54] See Supplemental Material of Ref. [42].
[55] N. Kawashima and Y. Tanabe, Phys. Rev. Lett. **98**, 057202 (2007).
[56] T. Okubo, K. Harada, J. Lou, and N. Kawashima, Phys. Rev. B **92**, 134404 (2015).
[57] Zero-temperature projector variants of the resummed SSE algorithm in higher-symmetric representations can also now be envisaged.
[58] K. Beach and A. W. Sandvik, Nucl. Phys. B **750**, 142 (2006).
[59] See in particular Sec. III A of Ref. [37].
[60] See in particular Sec. III D of Ref. [37].
[61] A. W. Sandvik, Phys. Rev. Lett. **98**, 227202 (2007).
[62] T. Senthil, A. Vishwanath, L. Balents, S. Sachdev, and M. P. A. Fisher, Science **303**, 1490 (2004).
[63] T. Senthil, L. Balents, S. Sachdev, A. Vishwanath, and M. P. A. Fisher, Phys. Rev. B **70**, 144407 (2004).
[64] In Ref. [38], the underlying lattice of the classical loop gas is the so-called "3D L lattice" (Fig. 1 of Ref. [38]), while it is the JQ model on square lattice maps to a loop gas on a simple cubic lattice. Such a difference is expected to not affect the long-distance universal physics, since both lattices have the same cubic symmetry. The same goes for the microscopic differences in the transfer matrices.